

# RegistrationMamba: A Mamba-based Registration Framework Integrating Multi-Expert Feature Learning for Cross-Modal Remote Sensing Images

Wei Wang, Dou Quan, *Member, IEEE*, Chonghua Lv, *Student Member, IEEE*, Shuang Wang, *Senior Member, IEEE*, Ning Huyan, *Member, IEEE*, Yunan Li, *Member, IEEE*, Licheng Jiao, *Fellow, IEEE*

**Abstract**—Cross-modal remote sensing image (CRSI) registration is critical for multi-modal image applications. However, CRSI mainly faces two challenges: significant nonlinear radiometric variations between cross-modal images and limited textures hindering the discriminative information extraction. Existing methods mainly adopt convolutional neural networks (CNNs) or Transformer architectures to extract discriminative features for registration. However, CNNs with the local receptive field fail to capture global contextual features, and Transformers have high computational complexity and restrict their application to high-resolution CRSI. To solve these issues, this paper proposes RegistrationMamba, a novel Mamba architecture based on state space models (SSMs) integrating multi-expert feature learning for improving the accuracy of CRSI registration. Specifically, RegistrationMamba employs a multi-directional cross-scanning strategy to capture global contextual relationships with linear complexity. To enhance the performance of RegistrationMamba under texture-limited scenarios, we propose a multi-expert feature learning (MEFL) strategy to capture features from various augmented image variants through multiple feature experts. MEFL leverages a learnable soft router to dynamically fuse the features from multiple experts, thereby enriching feature representations and improving registration performance. Notably, MEFL can be seamlessly integrated into various frameworks, substantially boosting registration performance. Additionally, RegistrationMamba integrates a multi-level feature aggregation (MFA) module to extract fine-grained local information and enable effective interaction between global and local features. Extensive experiments on CRSI with varying image resolutions have demonstrated that RegistrationMamba has superior performance and robustness compared to state-of-the-art methods.

**Index Terms**—Cross-modal images, image registration, mamba, multi-expert, feature learning

## I. INTRODUCTION

REMOTE sensing image registration is widely used for multi-modal image fusion [1] and multi-temporal image change detection [2]. It aims to accurately align images captured by different sensors, at different times, or from different viewpoints [3], [4].

Due to the complementary characteristics, cross-modal image registration based on optical and Synthetic Aperture Radar (SAR) images attracted a large number of researchers' attention. Optical images rely on visible or near-infrared

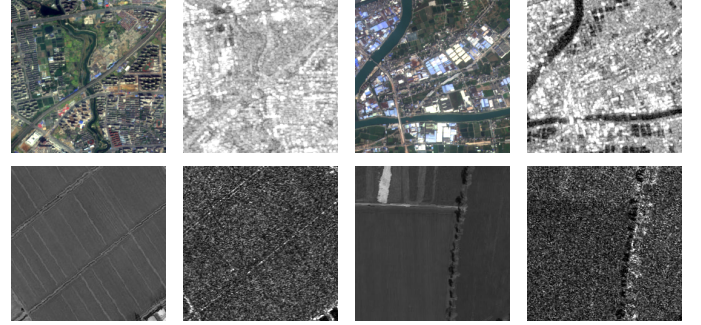


Fig. 1. Example images from the SEN1-2 dataset with 10-meter resolution and the OS dataset with 1-meter resolution. Top row: SEN1-2 dataset. Bottom row: OS dataset. Left column: Optical images. Right column: SAR images.

spectrum reflection to display surface features (e.g., vegetation, buildings, and water), providing high spatial resolution and rich color information. However, they are susceptible to poor illumination conditions. SAR images capture object scattering characteristics through electromagnetic wave reflection. These images can penetrate atmospheric obstacles (e.g., clouds and haze) while acquiring effective nighttime observations.

Current remote sensing systems can eliminate significant geometric transformations, such as rotation and scaling, through radiometric correction based on sensor calibration parameters. Therefore, existing image registration methods focus on accurately aligning images with slight translations. Following this line of research, image registration approaches fall into two categories. Feature-based registration focuses on extracting local discriminative features that are invariant to image transformation and illumination changes, such as scale-invariant feature transform (SIFT) [5]. Region-based methods, also named template matching methods [6], search for the matching location by maximizing similarity metrics, such as normalized cross-correlation (NCC) [7], and mutual information (MI) [8]. Feature-based methods struggle to extract discriminative local features and obtain sufficient matching points for image registration in remote sensing images with poor textures or highly repetitive local patterns. In contrast, Region-based methods, which leverage global feature information from images, demonstrate stronger robustness compared to local feature-based approaches. Therefore, this paper focuses on improving region-based methods for image registration. To address the differences between cross-modal images, existing studies adopt structural similarity descriptors for cross-modal

Wei Wang, Dou Quan, Chonghua Lv, Shuang Wang, and Licheng Jiao are with the Key Laboratory of Intelligent Perception and Image Understanding of Ministry of Education of China, Yunan Li is with the School of Computer Science, Xidian University, Xi'an 710071, China. Ning Huyan is with the Department of Automation, Tsinghua University, Beijing 100084, China.

registration [9], [10]. Nevertheless, their performance remains limited when handling images with significant modality gaps.

Recently, deep learning-based methods have demonstrated significant advantages over traditional handcrafted approaches for remote sensing image registration. They employ deep convolutional neural networks (CNNs) [3], [11] to learn shared cross-modal features. Existing approaches aim to enhance registration performance through multiple strategies. For instance, expanding receptive fields via dilated convolutional operators to capture richer contextual information [12], preserving spatial details through multi-scale feature learning networks [13], [14], implementing coarse-to-fine registration using two-stage frameworks [15], [16], enhancing feature discriminability by incorporating frequency-domain information [17], combining handcrafted features with deep representations for improved accuracy [18], [19]. Despite these innovations, three critical limitations persist. Firstly, CNN-based methods fail to capture global contextual relationships due to their inherent local connectivity, particularly under texture-poor scenarios or repetitive pattern conditions. Secondly, while Transformer architectures can address global feature extraction, they incur prohibitive computational costs when processing high-resolution remote sensing imagery. Additionally, the registration performance of the deep learning-based method will degrade significantly in low-texture scenarios (see the bottom row of Fig. 1), as networks struggle to extract discriminative features from information-sparse local regions.

To solve these challenges, this paper proposes a RegistrationMamba with multi-expert feature learning for CRSI registration. We first introduce the Mamba architecture, based on state space models (SSMs) [20], into the CRSI registration task. Although the Mamba framework has been successfully applied to hyperspectral image classification [21] and change detection [22], its potential for CRSI registration remains unexplored. Our proposed RegistrationMamba achieves two key advantages: Global context modeling with linear complexity through multidirectional cross-scanning strategies; Effective extraction of global contextual features while maintaining low computational overhead for accurate image registration. Furthermore, inspired by Mixture of Experts (MoE) [23]–[26], we propose a multi-expert feature learning strategy (MEFL) to improve image registration performance under texture-limited scenarios. Specifically, MEFL adopts different affine transformations to the input images and extracts salient information using multiple experts from various augmented image variants. It dynamically aggregates this information through a learnable soft router, resulting in richer and more discriminative features. MEFL can be seamlessly integrated with various model architectures (such as CNNs and ViTs) and achieves effective performance gains. Furthermore, we introduce a Multi-level Feature Aggregation (MFA) module into the encoder to adaptively fuse global contextual information with local texture details, significantly enhancing registration accuracy.

The main contributions of this paper are as follows:

- We propose a **RegistrationMamba**, a cross-modal remote sensing image registration module based on the Mamba framework with multi-expert feature learning.

RegistrationMamba can capture global contextual information with linear computation complexity for more accurate image registration.

- This paper designs a general multi-expert feature learning strategy (MEFL) to improve the registration performance under texture-limited scenarios. MEFL enriches feature representations by performing multi-expert feature learning and dynamic aggregation on image features under different augmented variants. MEFL can be easily and quickly integrated into different frameworks and yields significant performance improvements.
- Experimental results on optical and SAR images with various image resolutions from the OSdataset and SEN1-2 dataset have shown the effectiveness and advantages of the proposed RegistrationMamba on cross-modal image registration. It outperforms existing state-of-the-art methods.

## II. RELATED WORKS

### A. Cross-Modal Remote Sensing Image Registration

CRSI registration approaches can be classified into two categories: traditional methods and deep learning-based methods.

**Traditional Methods:** Traditional methods are generally divided into feature-based and region-based methods depending on their registration processes. Feature-based methods [5], [27] aim to extract invariant features and achieve registration by establishing local correspondences through similar local descriptors between remote sensing images. Region-based methods (also known as template matching) involve sliding template windows pixel-by-pixel over reference images while maximizing similarity metrics such as normalized cross-correlation (NCC) [7] and mutual information (MI) [28]. Moreover, Ye et al. proposed the CFOG descriptor [10], which enhances the discriminative power and robustness of image structural features through multi-directional pixel gradient features, thereby improving both registration accuracy and computational efficiency.

**Deep Learning Methods:** Due to the strong ability of feature learning, deep learning-based methods have achieved breakthrough advances in remote sensing tasks, such as change detection [2], semantic segmentation [29], [30], and cross-modal fusion [31]. Deep learning methods also exhibit significant advantages over traditional hand-crafted descriptors on remote sensing image registration [32]. Typical registration frameworks [6], [12], [33], [34] employ Siamese-based CNN architectures to extract shared discriminative features from multi-modal images, effectively facilitating image matching and alignment through learned feature correspondences. Existing methods further boost image registration performances from the following perspectives: 1) expanding receptive fields, 2) fusing multi-level or multiple features, 3) introducing frequency-domain information, and 4) adopting coarse-to-fine frameworks. Firstly, [12] uses dilated convolutional operators to expand receptive fields and capture rich contextual information for improving registration performances. Secondly, the multi-level features or multiple features are used for improving image registration performance. AFD-Net [35] proposes a

multi-level feature difference aggregation strategy, improving feature distinguishability. AESF [18] introduces a hybrid registration method that employs attention mechanisms to enhance structural features, thereby combining the advantages of both handcrafted and deep learning-based methods to improve registration performance. MOPSI [19] combines phase structure convolutional features with a multi-scale fusion network to address nonlinear radiometric differences. Additionally, several works introduce the frequency information to augment the feature representation for image registration. F3Net [17] proposes an adaptive frequency filtering network to select important frequency components and capture non-local contextual information for cross-modal image registration. DW-Net [36] combines the multi-resolution wavelet features and deep features for improving cross-modal image registration. FFT U-Net [37] and MARU-Net [14] combined Siamese U-Net structures [30] with Fast Fourier Transform (FFT)-based correlation, leveraging the frequency domain for efficient similarity computation. Moreover, the two-stage framework based on coarse-to-fine image registration is used to achieve more accurate registration results. MU-Net [38] conducts coarse-to-fine hierarchical image registration based on various image resolutions. RSOMNet [15] effectively improves the accuracy and generalization ability of registration through multi granularity feature alignment and non-shared content filtering. GLS-MIFT [16] combines global-to-local search and adaptive rotation-invariant descriptors to maintain high accuracy and robustness under severe nonlinear radiation distortion.

However, the cross-modal registration results still need to be improved. CNN-based methods suffer from restricted receptive fields that hinder rich spatial context modeling. Transformer-based methods achieve global feature interaction but incur prohibitive computational costs for high-resolution images. Additionally, when the image scenes with limited texture features, their performance drops sharply. In this paper, we propose RegistrationMamba based on state space models (SSMs) for CRSI registration. RegistrationMamba has linear complexity and global modeling capabilities, which can boost registration performances without bringing expensive computational costs. Furthermore, we propose a multi-expert feature learning strategy (MEFL) to further improve the registration performance of images under texture-limited scenarios. MEFL aims to capture richer features through multiple expert learning and dynamically aggregates based on various augmented images.

### B. State Space Models

Mamba is a deep learning architecture based on state space models (SSMs), which combines RNN's recursive properties and Transformer's parallel computation, enabling the capture of global contextual information with lower computational complexity. Visual Mamba [39] extends the Mamba architecture for computer vision tasks and builds a vision backbone with bidirectional Mamba blocks, achieving significant advantages in computation efficiency. It uses bidirectional state space models to acquire visual features for image classification, object detection, and semantic segmentation tasks.

The Mamba framework has been preliminarily applied to remote sensing image processing tasks including hyperspectral image classification, change detection, and image super-resolution [40]. For example, DTAM [41] proposes a dynamic token augmentation mamba, which unfolds hyperspectral images (HSI) into long sequences and captures global features for cross-scene HSI classification. HyperMamba [21] proposes a spectral-spatial adaptive Mamba for HSI classification. HyperMamba performs spectral scanning and enhances the spectral features using neighborhood spectral information for high-precision HSI classification. ChangeMamba [22] explores the potential of the Mamba architecture for remote sensing change detection. It utilizes the Visual Mamba to extract the global spatial contextual information from the input images, obtaining accurate change results. ConMamba [42] builds a hybrid encoder based on CNN and SSM for image change detection, which can dynamically integrate CNN's local detail features with Mamba's global dependency modeling capability through feature interaction. MF-VMamba [43] introduces the Mamba architecture to the remote sensing image change detection task, breaking the traditional CNN and Transformer bottlenecks in global modeling and computational efficiency through multi-scale feature extraction and fusion mechanisms. RS-Mamba [44] effectively captures large-scale spatial features in various directions from high-resolution remote sensing images and presents effectiveness on semantic segmentation and change detection tasks.

Although the Mamba framework has been applied to various remote sensing image tasks, its potential in remote sensing image registration has yet to be explored. In the CRSI registration task, it is crucial to capture the global contextual information to enhance registration accuracy and maintain high efficiency. This paper first explores the capability of the Mamba framework in image registration and proposes RegistrationMamba. RegistrationMamba can model long-range global dependencies with linear computational complexity by adopting a multi-directional cross-scan strategy in each feature extraction stage, thereby effectively enhancing registration performance. Furthermore, we introduce a multi-level feature aggregation module in the encoder, which adaptively fuses global contextual information and local texture details to improve registration performance further.

### C. Mixture of Experts

The Mixture of Experts (MoE) [23], [45] adopts the Divide-and-Conquer idea, which decomposes a task into multiple sub-tasks and jointly trains a set of specialized models, referred to as "experts". Specifically, MoE usually consists of multiple homogeneous expert models and a trainable routing network. The router employs sparse gating and assigns a score to each expert to select a small number of experts, reducing the computational costs [46], [47].

MoE has been introduced into many remote sensing image tasks, such as image super-resolution [48], image captioning [49], image fusion [50], object tracking [51], and image dehazing [52]. For instance, [48] uses a set of experts to deal with diverse ground objects and complex details in remote sensing

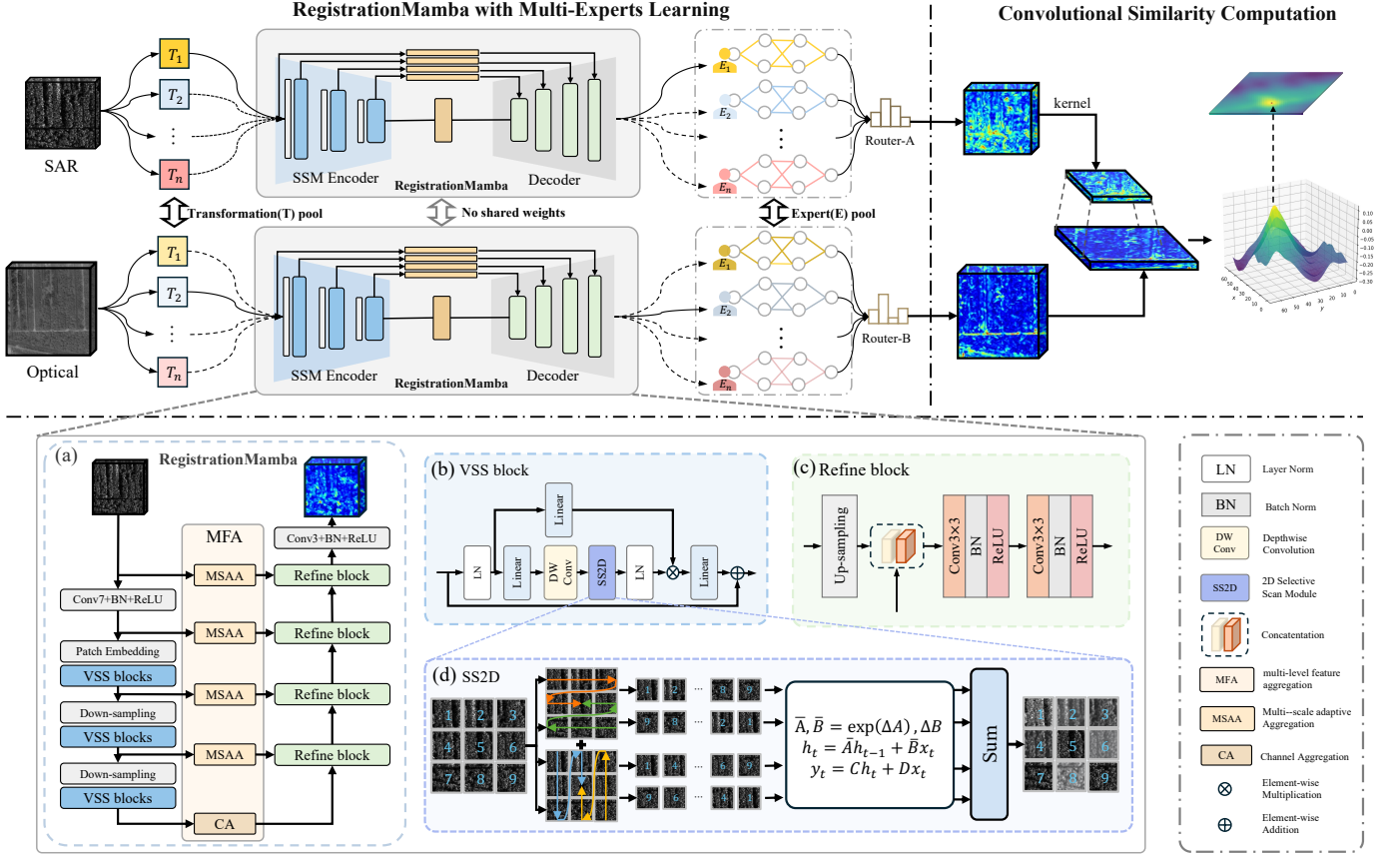


Fig. 2. The framework of the RegistrationMamba with multi-expert feature learning. RegistrationMamba uses a Mamba-based framework to extract features from input images. Additionally, RegistrationMamba adopts multi-expert feature learning (MEFL) to enhance feature richness through various image transformations and multi-expert feature aggregation. Finally, we find the matching location by computing the similarity map of the optical and SAR features.

images, improving the performance of remote sensing image super-resolution. MoE-Fusion [50] mixes local and global experts and proposes a hierarchical expert dynamic fusion mechanism for the adaptive fusion of infrared and visible images. HotMoE [51] introduces the MoE to hyperspectral object tracking. It employs a dynamic routing-driven sparse expert selection strategy to reduce the computational complexity. Additionally, HotMoE can enhance the tracking performance by combining the capabilities of different experts. SFAN [52] proposes a spatial-frequency adaptive network for image dehazing, which uses a mixture of fusion experts to enhance the low-frequency and high-frequency feature interaction.

Existing methods mainly focus on leveraging the sparsity and dynamics of MoE to integrate the knowledge of multiple experts and reduce computational costs. Inspired by MoE, this paper proposes a multi-expert feature learning (MEFL) approach for CRSI registration. MEFL aims to capture rich and robust features, boosting the registration performance for images with limited textures. Unlike existing sparse expert-selection paradigms prioritizing computational efficiency, our MEFL focuses on feature fusion of various affine-transformed images via a learnable soft router.

### III. METHODOLOGY

This paper proposes RegistrationMamba for cross-modal remote sensing image registration, which combines the Mamba

framework with multi-expert feature learning. As illustrated in Fig. 2, RegistrationMamba mainly comprises three core components. Firstly, RegistrationMamba uses a feature extractor based on the Mamba framework for global feature extraction, providing discriminative feature representations for image registration. Secondly, RegistrationMamba adopts multi-expert feature learning (MEFL) to enhance feature richness. MEFL first performs various affine transformations on the input images and designs multiple experts to capture various significant features from these transformed images. After that, MEFL aggregates the features of multiple experts using a learnable soft router for image matching. Finally, we compute the similarity map of the optical and SAR features and match cross-modal images.

#### A. Preliminaries

State space models (SSMs) are mathematical modeling approaches that center around the system's state and describe the behavior and evolution of dynamic systems over time. They are widely applied in control systems, time series analysis, and signal processing. Mamba and a series of models based on SSMs are inspired by linear time-invariant systems, which describe the continuous dynamics of a system using ordinary differential equations (ODEs). These ODEs map the input



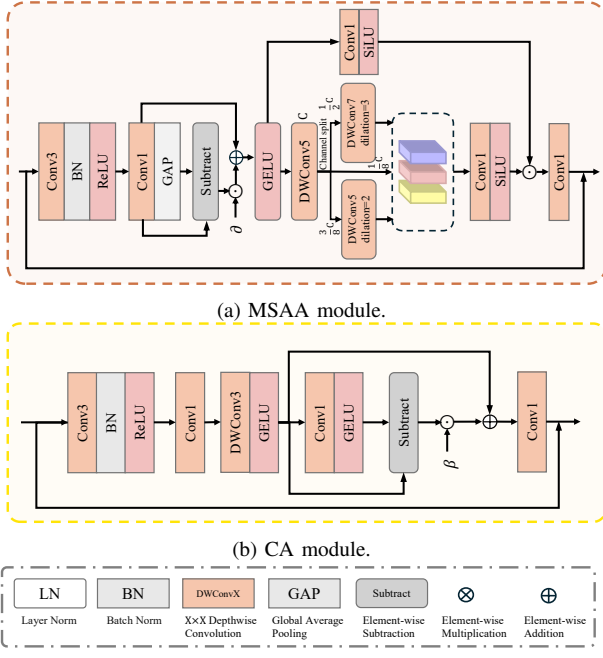


Fig. 3. The multi-level feature aggregation (MFA) module. MFA module comprises two sub-modules: multi-scale adaptive aggregation (MSAA) and channel aggregation (CA). MSAA is designed to further adaptively extract multi-scale local features from the global features captured at each level of the SSM encoder. CA is applied exclusively to the deepest semantic features, performing lightweight channel aggregation to enhance the representation capability of high-level features.

signal to a latent space. Mathematically, it can be expressed as:

$$\begin{cases} h'(t) = \mathbf{A}h(t) + \mathbf{B}x(t), \\ y(t) = \mathbf{C}h(t) + \mathbf{D}x(t), \end{cases} \quad (1)$$

where  $x(t) \in \mathbb{R}$  represents the input sequence signal,  $y(t) \in \mathbb{R}$  represents the output signal, and  $h(t) \in \mathbb{R}^N$  represents the latent state.  $h'(t) \in \mathbb{R}^N$  denotes the time derivative of  $h(t)$ . Additionally,  $\mathbf{A} \in \mathbb{R}^{N \times N}$  acts as the state transition matrix,  $\mathbf{B} \in \mathbb{R}^{N \times 1}$  and  $\mathbf{C} \in \mathbb{R}^{1 \times N}$  are projection matrices,  $\mathbf{D} \in \mathbb{R}^1$  commonly acts as a residual connection. Specifically, the parameter  $\mathbf{A}$  stores historical information, and  $\mathbf{B}$  controls the influence of the current input  $x(t)$  on the hidden state. The output  $y$  is generated by a combination of the hidden state and the input  $x(t)$ .

In Mamba [20], the ordinary differential equations are discretized using a zero-order hold (ZOH), and the continuous parameters  $\mathbf{A}$  and  $\mathbf{B}$  are transformed into discrete parameters  $\bar{\mathbf{A}}$  and  $\bar{\mathbf{B}}$  via a time-scale parameter  $\Delta$ , which can be expressed as:

$$\begin{cases} \bar{\mathbf{A}} = \exp(\Delta \mathbf{A}), \\ \bar{\mathbf{B}} = (\Delta \mathbf{A})^{-1}(\exp(\Delta \mathbf{A}) - \mathbf{I}) \cdot \Delta \mathbf{B}. \end{cases} \quad (2)$$

After discretization, the system can be expressed as:

$$\begin{cases} h'_t = \bar{\mathbf{A}}h_{t-1} + \bar{\mathbf{B}}x_t, \\ y_t = \mathbf{C}h_t. \end{cases} \quad (3)$$

To enhance computational efficiency, the sequence  $x$  with length  $N$  can be computed using a global convolution to

produce the output  $y$ . The specific equation can be expressed as:

$$\begin{cases} \bar{\mathbf{K}} = (\bar{\mathbf{C}}\bar{\mathbf{B}}, \bar{\mathbf{C}}\bar{\mathbf{A}}\bar{\mathbf{B}}, \bar{\mathbf{C}}\bar{\mathbf{A}}^2\bar{\mathbf{B}}, \dots, \bar{\mathbf{C}}\bar{\mathbf{A}}^{N-1}\bar{\mathbf{B}}), \\ y = x * \bar{\mathbf{K}}, \end{cases} \quad (4)$$

where  $*$  denotes the convolution operation, and  $\bar{\mathbf{K}}$  represents the convolution kernel. However, the traditional SSM is linear and time-invariant, meaning that the projection matrices do not change with the input. This limitation prevents the model from considering the importance of different time steps. Mamba addresses this by using a selective scanning mechanism, mapping the parameter matrices as:

$$\begin{cases} \bar{\mathbf{B}} = s_B(x), \\ \bar{\mathbf{C}} = s_C(x), \\ \Delta = \tau_\Delta(\Theta + s_\Delta(x)). \end{cases} \quad (5)$$

where  $\Theta$  is a randomly selected set of values, the model dynamically adjusts its parameters based on the input. It transforms the SSM into a linear time-varying system, thereby improving its performance in processing complex sequences.

### B. RegistrationMamba for feature learning

Given a template image (SAR image) and a reference image (optical image), we aim to locate the position in the reference image that matches the template image. We employ the RegistrationMamba to extract features for image matching. Figure 2 illustrates the framework of the proposed RegistrationMamba for cross-modal remote sensing image registration. Unlike 1D language sequences, 2D visual data requires greater attention to spatial information. Inspired by VMamba [53], the RegistrationMamba integrates visual state space (VSS) blocks as the fundamental feature encoding module.

Suppose the input gray optical image is  $X_O \in \mathbb{R}^{H_o \times W_o \times 1}$  and SAR image is  $X_S \in \mathbb{R}^{H_s \times W_s \times 1}$ , we adopt the RegistrationMamba with modality-specific weights to extract features from optical and SAR images, respectively, effectively adapting to cross-modal differences. The feature extraction can be divided into three stages. The first stage is global context feature extraction, where a multi-directional cross-scanning strategy based on a state space model is employed to capture spatial global contextual information from images. The second stage is multi-level feature aggregation, where multi-scale adaptive aggregation and channel aggregation are utilized to enhance local feature learning. The third stage is feature refinement, where global and local features at each level effectively interact and fuse to improve feature discrimination.

1) *Global context feature extraction*: Taking input image  $X_S \in \mathbb{R}^{H \times W \times 1}$  as an example, we first use a convolutional block with a convolutional kernel size of  $7 \times 7$  to extract feature  $F_0$  from  $X_S$ . After that, we segment the feature map into patches and project them into a sequence input  $F'_0 \in \mathbb{R}^{\frac{H}{P} \times \frac{W}{P} \times D}$ , where  $P$  represents the patch size and  $D$  the latent dimension. Next, we adopt several VSS blocks to model the spatial contextual information. A downsampling operation is used between each level. As shown in Fig. 2(a), we can acquire hierarchical feature representations  $F'_i$ , where  $i \in \{0, 1, 2, 3\}$ .

The structure of the VSS block is depicted in Fig. 2(b). The input feature is first processed through a layer normalization and then split into two branches. One branch contains a linear embedding layer, followed by a  $3 \times 3$  depth-wise convolution (DWConv) layer, a 2D selective scanning module (SS2D) for contextual modeling, and a layer normalization. The other branch contains a linear embedding layer. The outputs of both branches are fused with the input feature via residual connection to produce the final output. In SS2D, we encode image patch sequences from four different directions, creating four distinct sequences. Each sequence is processed using SSM, and the final feature map is obtained by merging output features from all four sequences. As shown in Fig. 2(d), suppose the input of the SS2D is  $f$ , the output  $f'$  can be expressed as follows:

$$\begin{cases} f_j = \text{Expand}(f, j), \\ f_j = S6(f_j), \\ f' = \text{Merge}(\bar{f}_1, \bar{f}_2, \bar{f}_3, \bar{f}_4), \end{cases} \quad (6)$$

where  $\text{Expand}(\cdot)$  denotes the scanning expansion (creating sequences based on scanning directions),  $j \in \{1, 2, 3, 4\}$  corresponds to the four different scanning directions. The selective cross-scanning spatial state sequential model  $S6$  serves as the core operator, enabling each pixel in the image to effectively integrate information from all pixels across different directions.  $\text{Merge}(\cdot)$  indicates the scanning merging process (adding the sequences processed by the  $S6$  module from different scanning directions and reshaping the result into a 2D feature map).

2) *Multi-level feature aggregation*: In the second stage, we utilize a multi-level feature aggregation (MFA) module to extract multi-scale local features or high-level feature representations from the global contextual features at each level.

$$\begin{cases} Z = MFA(X_S), \\ Z_i = MFA(F'_i), i = 0 \dots 3, \end{cases} \quad (7)$$

where  $MFA$  represents the multi-level feature aggregation operator.

MFA module uses two components: multi-scale adaptive aggregation module (MSAA) and channel aggregation module (CA). These two modules are used at different stages of the network, where MSAA is mainly responsible for multi-scale feature aggregation and CA focuses on high-level feature channel aggregation. As shown in Fig. 3(a), MSAA module comprises a series of depth-wise convolutions at different scales. We fuse these multi-scale features and input features through an element-wise multiplication operation. MSAA extracts multi-scale features with adaptive local perception, enhancing fine-grained local texture information extraction. For the input feature  $F'_i$ , the details of the MSAA are as follows:

$$\begin{cases} Y_i = \text{Conv}_1(\text{ReLU}(\text{BN}(\text{Conv}_3(F'_i))))), \\ Y'_i = \text{GELU}(Y_i + \alpha \odot (Y_i - \text{GAP}(Y_i))), \\ \bar{Y}_i = \text{DWConv}_5(Y'_i), \\ Z'_i = \text{Cat}(\delta_1 \text{DWConv}_5(\bar{Y}_i), \delta_2 \text{DWConv}_7(\bar{Y}_i), \delta_3 \bar{Y}_i), \\ \bar{Z}_i = \text{SiLU}(\text{Conv}_1(Z'_i)) \odot \text{SiLU}(\text{Conv}_1(Y'_i)), \\ Z_i = F'_i + \text{Conv}_1(\bar{Z}_i), \end{cases} \quad (8)$$

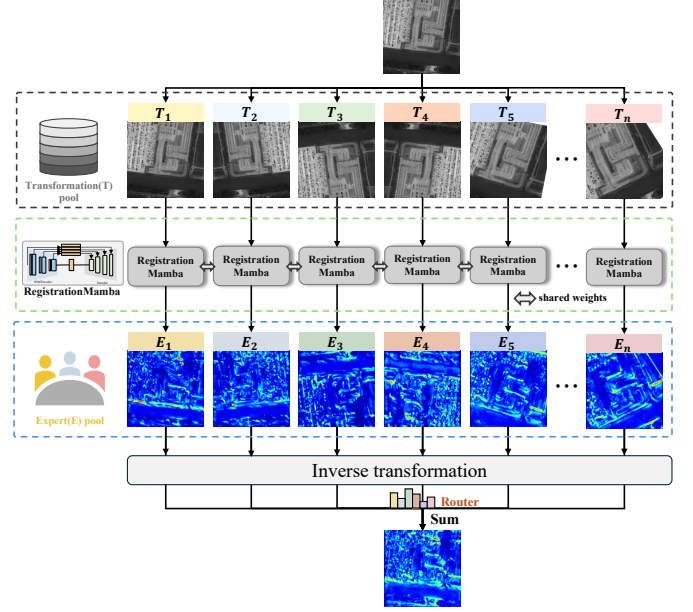


Fig. 4. The proposed multi-expert feature learning (MEFL) strategy. We randomly apply several geometric transformations to the input image in the image transformation pool, and then use RegistrationMamba to extract features from various transformed images. For each image feature, we select corresponding experts in the expert pool, and each expert focuses on extracting salient information from the features of different transformations. Finally, expert routers are used to adaptively fuse the features after inverse transformation, resulting in the final rich feature representation.

where  $\alpha$  denotes the scaling factor,  $\delta_1$ ,  $\delta_2$ , and  $\delta_3$  denote the proportions used to partition the features along the channel dimension, which are  $\frac{3}{8}$ ,  $\frac{1}{2}$ ,  $\frac{1}{8}$ , respectively, Cat denotes the concatenation operation,  $\text{Conv}_l$  represents a convolution with a kernel size of  $l \times l$ , and  $\text{DWConv}_l$  represents a depthwise convolution with a kernel size of  $l \times l$ .

Meanwhile, for the high-level features  $F'_3$ , we employ a CA module to reassign channel features within the high-dimensional latent space dynamically. CA module improves both channel efficiency and feature representation compared to classical channel augmentation [31], all while maintaining a small increase in network parameters and computational cost. The details of the CA are as follows:

$$\begin{cases} Y_3 = \text{Conv}_1(\text{ReLU}(\text{BN}(\text{Conv}_3(F'_3))))), \\ \bar{Y}_3 = \text{GELU}(\text{DWConv}_3(Y_3)), \\ Z'_3 = \bar{Y}_3 + (\bar{Y}_3 - \beta \odot (\text{GELU}(\text{Conv}_1(\bar{Y}_3))))), \\ Z_3 = F'_3 + \text{Conv}_1(Z'_3), \end{cases} \quad (9)$$

where  $\beta$  denotes the scaling factor.

3) *Feature refinement*: To enhance feature representation, we fuse multi-level information, including global information and fine-grained local information at each level. Specifically, as shown in Fig. 2(c), we first upsample the features from the previous level and concatenate them with the features of the MFA module. Then, we perform adaptive fusion and refinement, generating the final fused feature for image registration,  $F_S$ .

### C. Multi-expert feature learning

Although deep features exhibit strong invariance to image modality changes, their performance on texture-limited images requires further improvement. To address this issue, we propose a multi-expert feature learning (MEFL) strategy to enhance the deep model's ability to capture richer feature representations by aggregating the features from various transformations of the input image. Specifically, we design an image transformation pool and a corresponding expert pool. In the image transformation pool, we apply arbitrary geometrical transformations to image pairs, including flipping, random rotation, and homography transformation. Then, we use RegistrationMamba to extract features from transformed images. For each transformed image feature, we select the corresponding expert from the expert pool. Each expert specializes in extracting salient information from the features of different transformations.

The extracted features of different transformed images are recalibrated through the corresponding inverse transformation. Unlike traditional MoE approaches that sparsely select expert features for fusion [54], we adaptively fuse the features of all experts through a learnable soft router, enriching the feature representation and enhancing the discrimination of features. The detail of MEFL can be represented as follows:

$$X_S^n = T_n(X_S), \quad (10)$$

$$F_S^n = \text{RegistrationMamba}(X_S^n), \quad (11)$$

$$\bar{F}_S^n = E_n(F_S^n), \quad (12)$$

$$w_i = \text{softmax}(\alpha_i) = \frac{e^{\alpha_i}}{\sum_{j=0}^{n-1} e_j^\alpha}, \quad (13)$$

$$F_S = \sum_{i=0}^{n-1} w_i \cdot \bar{F}_S^i, \quad (14)$$

where  $T_n$  represents the  $n_{th}$  image transformation from the image transformation pool,  $E_n$  denotes the  $n_{th}$  expert from the feature expert pool,  $X_S$  denotes the input image (using the template image as an example),  $\bar{F}_S^n$  refers to the features extracted by different experts,  $\alpha_i$  represents the learnable soft router parameters, and  $F_S$  is the aggregated feature from various experts.

It should be noted that the proposed MEFL strategy exhibits strong generalizability and can be seamlessly integrated into various frameworks, significantly improving the performance of cross-modal image registration.

### D. Similarity computation and loss function

1) *Similarity computation*: The similarity calculation between the template and the reference image based on the pixel-by-pixel comparison is highly time-consuming and significantly increases training and inference times. To accelerate this process, we employ a convolution-based similarity computation method. Specifically, the feature map of the template image is used as a convolution kernel and convolved with the feature map of the reference image. Since convolution operations can be efficiently parallelized on GPUs, this approach substantially improves the speed of both training and inference.

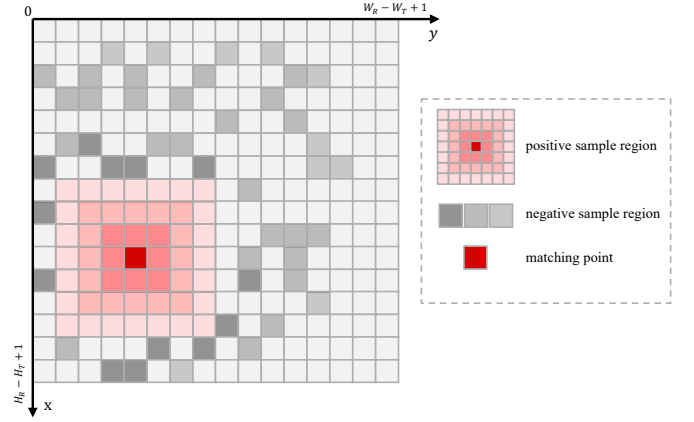


Fig. 5. The similarity map. The red grid represents the positive locations, where the center indicates the ground truth of the matching location. The gray region represents the negative locations.

The similarity computation can be represented as follows:

$$F[i, j] = \sum_{c=1}^C \sum_{k=1}^{H_S} \sum_{l=1}^{W_S} F_S[c, k, l] \cdot F_O[c, i+k, j+l], \quad (15)$$

$$\text{Sim}[i, j] = \frac{F[i, j]}{\|F_S\|_2 \cdot \|F_O\|_2}. \quad (16)$$

where  $\text{Sim}[i, j]$  represents the feature similarity of the template image  $X_S$  at position  $(i, j)$  in the reference image  $X_O$ ,  $F_S \in \mathbb{R}^{C \times H_S \times W_S}$  denotes the feature map of the template image,  $F_O \in \mathbb{R}^{C \times H_O \times W_O}$  denotes the feature map of the reference image, and the size of the similarity map is  $(H_O - H_S + 1) \times (W_S - W_S + 1)$ .

2) *Loss Function*: Following [17], this paper also employs three loss functions for network optimization: the matching loss,  $L_m$ , the fine similarity loss,  $L_{fine}$ , and the similarity peak loss,  $L_{peak}$ .

**Matching loss**: As illustrated in Fig. 5, we treat the matching point and a small surrounding region as positive samples, while the region with the highest similarity outside the matching area is treated as a negative sample. The matching loss can be represented as follows:

$$L_m = (S_{neg} + 1)^2 + (1 - S_{pos})^2. \quad (17)$$

where  $S_{pos}$  and  $S_{neg}$  represent the similarity of positive and negative samples, respectively. In this work, we select a  $7 \times 7$  region that surrounds the ground truth as the positive sample. For negative samples, we select  $topk$  samples with the highest similarity as negative sample locations for network optimization and  $k = 49$ .

**Fine similarity loss**: To further enhance the network optimization and find the accurate matching location, this paper uses the fine similarity loss for network training. It constrains the similarity values decrease gradually as the distance from the ground truth position increases. Fine similarity loss can be formulated as follows:

$$\begin{cases} G_{gt} = \text{Gaussian}(gt), \\ L_{fine} = (topk'(G_{gt}) - S_{pos}^{topk'})^2. \end{cases} \quad (18)$$

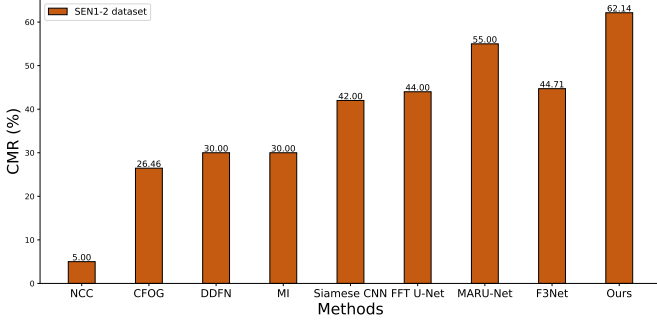


Fig. 6. The registration results of various methods at  $T = 1$  on the SEN1-2 dataset. The template image size is  $192 \times 192$ .

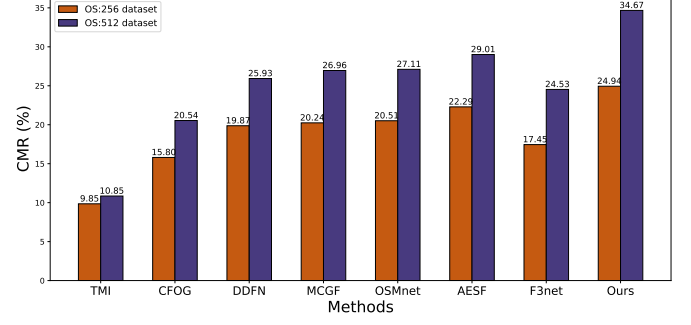


Fig. 7. The registration results of various methods at  $T = 1$  on the OS-256 and OS-512 datasets. Their template image sizes are  $192 \times 192$  and  $256 \times 256$ , respectively.

where  $G_{gt}$  represents the soft label region obtained by applying Gaussian smoothing to the ground truth location.  $S_{pos}^{topk'}$  denotes the subset of positive sample region corresponding to the  $topk'$  positions of  $G_{gt}$  and  $k' = 9$ .

**Similarity peak loss:** Additionally, this paper uses the similarity peak loss to constrain the similarity map to have a single peak at the matching location.

$$L_{peak} = 2 - (\max(S) - \text{mean}(S)). \quad (19)$$

where  $\max(\cdot)$  and  $\text{mean}(\cdot)$  denote maximum and average operators, respectively.

The final loss function for network optimization can be expressed as:

$$L_{final} = L_m + \gamma_1 L_{fine} + \gamma_2 L_{peak}. \quad (20)$$

where  $\gamma_1$  and  $\gamma_2$  denote the weight parameters corresponding to the losses, respectively.

#### IV. EXPERIMENTS AND RESULTS

In this section, we evaluate the effectiveness and advantages of the proposed RegistrationMamba for CRSI registration. Firstly, we introduce the datasets and experimental details. Secondly, we compare RegistrationMamba with existing representative methods for image registration. Subsequently, we conduct ablation studies to analyze the effectiveness of the multi-expert feature learning strategy and multi-level feature aggregation. Finally, we present the visualization of registration results and display the robustness of our proposal to noise.

##### A. Dataset

This paper tests the effectiveness of the proposal on two cross-modal image datasets, the SEN1-2 dataset and the OS dataset, which have different image resolutions.

**SEN1-2 dataset** [55] has 282,384 pairs of co-registered optical and SAR image patches acquired from Sentinel-1 and Sentinel-2 satellites. The image resolution is 10m, and the image size is  $256 \times 256$ . SEN1-2 dataset contains diverse land cover types (e.g., urban areas, plains, water bodies, deserts) and seasonal variations (spring, summer, autumn, winter). Following the experimental settings in [14], we select 6,450 image pairs from each season and acquire 25,800 pairs for

deep network training and testing. The ratio of the number of image pairs for training and testing is 7 : 3. Thus, there are 18,060 image pairs for training and 7,740 for testing. We randomly crop  $192 \times 192$  image patch from SAR images as the template, using the top-left coordinates of the cropped regions as the ground truth for matching.

**OS dataset** [56] also includes many SAR images and corresponding optical images. The SAR images are acquired using the multi-polarized C-band SAR satellite sensor GF-3 (Gaofen-3), while the optical images are obtained from the Google Earth platform. This dataset covers various cities and plain regions worldwide, such as Beijing and Shanghai in China, Guam and Tucson in the United States, and Agra in India. OS dataset contains 2,673 non-overlapping image pairs of size  $512 \times 512$  (labeled as OS-512) and 10,692 non-overlapping image pairs of size  $256 \times 256$  (labeled as OS-256). The image resolution is 1m. For the OS-512 dataset, we use 2,249 image pairs for training and 424 image pairs for testing and randomly crop  $384 \times 384$  image patches from the SAR images as template images. For the OS-256 dataset, we use 8,996 image pairs for training and 1,696 image pairs for testing and randomly crop  $192 \times 192$  image patches from the SAR images as template images.

The main challenges of these two datasets can be summarized as follows:

**Significant modality differences:** Due to the fundamentally different imaging principles between optical and SAR images, significant modality gaps exist. This makes it challenging for models to learn cross-modal invariant features and accurately identify registration regions simultaneously.

**Differences richness in local texture feature:** The SEN1-2 dataset has a resolution of 10m, whereas the OS dataset reaches 1m resolution. Within identically sized local receptive fields, the OS dataset likely contains fewer discriminative textures compared to SEN1-2, which significantly increases the difficulty of achieving precise alignment.

##### B. Evaluation Metrics

We use the  $L_2$  distance between the predicted matching location and the ground truth to evaluate the image registration accuracy. Additionally, we adopt the Correct Matching Rate (CMR) to assess the image registration performance. CMR



TABLE I

COMPARISON RESULTS OF THE AVERAGE  $L_2$  DISTANCE AND CMR ON THE SEN1-2 DATASET. THE TOP TWO RESULTS ARE MARKED AS RED AND BLUE, RESPECTIVELY.

Methods	$L_2 \downarrow$	CMR(T)(%) $\uparrow$			
		$T = 1$	$T = 2$	$T = 3$	$T = 5$
NCC [7]	31.60	5.00	11.00	16.00	23.00
CFOG [10]	-	26.46	40.67	49.79	-
DDFN [34]	17.50	30.00	42.00	50.00	55.00
MI [8]	11.80	30.00	45.00	54.00	62.00
Siamese CNN [12]	8.27	42.00	61.00	72.00	78.00
FFT U-Net [37]	6.92	44.00	63.00	74.00	80.00
MARU-Net [14]	4.94	55.00	75.00	82.00	87.00
F3Net [17]	4.15	44.72	81.03	87.24	89.97
Ours	2.93	62.14	82.25	89.19	93.04

TABLE II

COMPARISON RESULTS OF THE AVERAGE  $L_2$  DISTANCE AND CMR ON THE OS-512 DATASET. THE TOP TWO VALUES ARE MARKED AS RED AND BLUE.

Methods	$L_2 \downarrow$	CMR(T)(%) $\uparrow$			
		$T = 1$	$T = 2$	$T = 3$	$T = 5$
Him-net [57]	-	27.36	45.75	69.34	-
DC-InfoNCE [58]	-	34.67	58.96	78.30	92.69
F3Net [17]	3.18	24.53	51.18	72.41	89.62
Ours	2.39	34.67	61.32	80.42	94.58

represents the ratio of successful matches where the  $L_2$  distance between the predicted matching location and the ground truth is smaller than a given threshold  $T$ , denoted as  $CMR(T)$ . It can be formulated as:

$$CMR(T) = \frac{N_{match}}{N_{total}}, \quad (21)$$

$$L_2 = \sqrt{(x_p - x_g)^2 + (y_p - y_g)^2},$$

where  $N_{match}$  is the number of successful matching image pairs ( $L_2 \leq T$ ),  $N_{total}$  is the number of test image pairs,  $T$  is the distance threshold,  $(x_p, y_p)$  is the predicted matching position, and  $(x_g, y_g)$  is the corresponding ground truth.

### C. Implement Details

Our RegistrationMamba is implemented using the PyTorch framework and trained on Nvidia RTX 4090 GPUs. The AdamW optimizer is used to optimize the deep model, with a batch size of 4, an initial learning rate of 0.0005, and a training epochs of 10. This paper uses four experts in multi-expert feature learning. The feature extractor performs feature extraction at three feature scales, with each scale utilizing two cascaded VSS blocks. The output feature channels are 96, 192, and 384, respectively. In the loss function, both  $\gamma_1$  and  $\gamma_2$  are set to 1.

### D. Comparative experiments

This section compares the registration results of our RegistrationMamba with representative handcrafted and deep learning-based methods, including traditional template matching methods, i.e., NCC [7], MI [8], TMI [59] (Truncated MI),

CFOG [10], and deep feature learning methods, i.e., DDFN [34], Siamese CNN [12], FFT U-Net [37], MARU-Net [14], Him-Net [57], DC-InfoNCE [58], F3Net [17], and AESF [18].

Table I presents the registration performance of various methods on the SEN1-2 dataset. The proposed RegistrationMamba achieves the lowest average  $L_2$  distance and the highest registration accuracy (CMR) across different distance thresholds. Due to the significant differences between optical and SAR images, handcrafted methods have large registration errors. For example, the average  $L_2$  distance of MI is 11.80, and  $CMR(3)$  is 54.00%, respectively. Deep learning-based methods demonstrate significant advantages over traditional handcrafted methods. Specifically, MARU-Net achieves the average  $L_2$  distances of 4.94 and acquires the registration accuracy of 82.00% at  $T = 3$ . F3Net obtains the average  $L_2$  distances of 4.15 and has registration accuracy of and 87.24% at  $T = 3$ . These experimental results demonstrate that deep learning methods can better learn shared feature representations across image modalities.

Our proposed method outperforms all other methods, which acquires an average  $L_2$  distance of 2.93 and registration accuracy 89.19% at  $T = 3$ . Compared with FFT U-Net, MARU-Net and F3Net, our RegistrationMamba increases  $CMR(3)$  by 15.19%, 7.19%, and 1.95%, respectively.

Table II presents the registration performance of various methods on the OS dataset. DC-InfoNCE achieves a registration accuracy  $CMR(3)$  of 78.30%, while our method achieves  $CMR(3)$  of 80.42% and acquires a performance gain of 2.12%. Although the images in the OS dataset have limited textures in local regions, our proposed method still acquires better registration performance.

Existing advanced methods perform well in image registration tasks when scenes have rich texture features. For example, MARU-Net achieves a  $CMR(2)$  of 75.00% on the SEN1-2 dataset. However, most approaches are limited by the local receptive field inherent to CNN frameworks, making it difficult to capture global features that could improve registration accuracy. F3Net addresses this to some extent by introducing frequency domain information, which expands the receptive field and achieves a  $CMR(2)$  of 81.03% on the SEN1-2 dataset. Nevertheless, its performance is still restricted by the CNN structure. Transformer-based models can capture global information but come with high computational costs.

In contrast, our proposed RegistrationMamba can effectively capture global contextual information with linear complexity. It also aggregates multi-level features, enhancing the representation of local fine-grained features and improving feature discriminativeness. As a result, RegistrationMamba improves the  $CMR(2)$  on the SEN1-2 dataset by 1.22% compared to F3Net. Moreover, existing methods experience a significant performance drop on images with limited texture. For instance, F3Net's  $CMR(2)$  drops to only 51.18% on the OS-512 dataset. RegistrationMamba addresses this challenge by incorporating a multi-expert feature learning strategy. Different experts focus on distinct features under various affine transformations, and their outputs are aggregated using a router. This approach enables the model to learn rich features even in weakly textured scenes, leading to significantly improved registration

TABLE III  
ABLATION EXPERIMENTS ON THE OS-256 DATASET.

Base	RegistrationMamba	MEFL	$L_2 \downarrow$	CMR(T)(%) $\uparrow$		
				$T = 1$	$T = 2$	$T = 3$
✓			4.39	19.69	37.32	56.43
	✓		3.93	20.75	42.28	62.85
		✓	3.69	23.00	44.52	65.04
	✓	✓	3.39	24.94	48.11	67.92

TABLE IV  
ABLATION EXPERIMENTS ON THE MFA MODULE BASED ON THE OS-256 DATASET.

Model	$L_2 \downarrow$	CMR(T)(%) $\uparrow$		
		$T = 1$	$T = 2$	$T = 3$
W/O MSAA	3.65	23.82	45.34	65.57
W/O CA	3.46	24.41	45.70	66.63
W/O MSAA-CA	3.49	24.88	44.75	65.15
Ours	3.39	24.94	48.11	67.92

performance.

To further demonstrate the performance of our method in precise registration, we present the registration accuracy at  $T = 1$ , CMR(1), based on the SEN1-2 and OS datasets, as shown in Fig. 6 and Fig. 7. It can be seen that our proposed method achieves the best CMR(1) on the SEN1-2 and OS datasets. Specifically, on the SEN1-2 dataset, the best CMR(1) of the traditional handcrafted methods (MI) is 30.00%, the best CMR(1) of the deep feature learning methods (MARU-Net) is 55.00%, and the accuracy of our method is 62.14%. RegistrationMamba acquires performance gains of 32.14% and 7.14% compared to traditional and deep learning-based methods, respectively. On the OS-256 and OS-512 datasets, the best CMR(1) of traditional handcrafted methods (CFOG) are 15.80% and 20.54%, respectively. The best CMR(1) of deep feature learning methods (OSMNet) are 20.51% and 27.11%, respectively. AESF combines deep features and structural features, further improving registration performances. Its CMR(1) on the OS-256 and OS-512 datasets are 22.29% and 29.01%, respectively. Our proposed method achieves the best registration results, and its CMR(1) on the OS-256 and OS-512 datasets are 24.94% and 34.67%, respectively. Compared to AESF, the registration results are improved by 2.65% and 5.66%, respectively. The superior performance of our proposal is mainly attributed to the following aspects. Firstly, RegistrationMamba has strong feature representation ability, which can effectively capture global contextual information and local features. Secondly, RegistrationMamba uses multi-expert feature learning to capture salient information across different transformations, greatly enriching the feature representations for limited texture image registration.

#### E. Ablation Study of key modules

This section explores the effectiveness of the crucial modules in our proposed RegistrationMamba based on the OS-256 dataset, such as the Mamba framework and MEFL. Experimental results are presented in Table III. “Base” refers to the

U-shaped network based on the CNN framework. “MEFL” denotes the deep model that uses our proposed multi-expert feature learning strategy.

Experimental results in Table III demonstrate the effectiveness of our proposed Mamba framework and MEFL. Our Mamba framework acquires registration performance gains compared to the Base model. When using the Mamba framework alone, the average  $L_2$  decreases from 4.39 to 3.93, and the CMR(3) increases from 56.43% to 62.85%. When applying the MEFL strategy, the average  $L_2$  decreased to 3.69, and the CMR(3) increased to 65.04%. Our proposal combines the Mamba framework and MEFL strategy, and its average  $L_2$  decreases to 3.39, and CMR(3) increases to 67.92%.

#### F. Influence of the MFA

We also conduct ablation studies on the MFA (MSAA and CA modules) in RegistrationMamba, and the results are presented in Table IV. “W/O MSAA” and “W/O MSAA-CA” denote network does not contain the MSAA module and both the MSAA and CA modules, respectively.

The experimental results indicate that the MSAA and CA modules can enhance registration performance. Specifically, compared to our model with MSAA and CA, the “W/O MSAA”, “W/O CA”, and “W/O MSAA-CA” increase the average  $L_2$  by 0.26, 0.07, and 0.10, respectively, and decrease CMR(3) by 2.35%, 1.29%, and 2.77%, respectively.

The MSAA module adaptively extracts multi-scale features with local perception at each level in the encoder, enhancing the local texture information. The CA module adaptively reallocates channel features within the high-dimensional latent space. MFA, which combines the MSAA and CA modules, can encourage RegistrationMamba to effectively extract global contextual information while preserving the importance of local information, facilitating image registration performance.

#### G. Influence of the number of experts and fusion method in MEFL

This paper adopts the MEFL strategy to extract rich features from images and boost the registration performance of remote sensing images with limited textures. Thus, this section investigates the impact of the number of feature experts and the fusion method in the MEFL module based on the OS-256 dataset.

As shown in Table VI, “MEFL-0” denotes our RegistrationMamba without the MEFL strategy, and “MEFL-X” represent RegistrationMamba fuses features from the X experts. Compared to without the MEFL module, the MEFL module with multiple experts can significantly improve registration performance. Compared to the results of “MEFL-0”, the average  $L_2$  of “MEFL-4” is reduced by 0.54, and CMR(3) of “MEFL-4” is increased by 5.07%. Additionally, the more experts in the MEFL, the better the performance, when the number of experts increases from 2 to 4. However, as the model capacity further increases, the features extracted by multiple experts may become sufficient, causing the registration performance to gradually stabilize. Considering the registration accuracy

TABLE V

COMPARISON EXPERIMENTS ON THE OS-256 DATASET. “+MEFL” REPRESENTS THE DEEP MODEL THAT USES THE MULTI-EXPERT FEATURE LEARNING STRATEGY. THE BEST RESULTS ARE MARKED IN RED, AND THE PERFORMANCE GAINS ARE REPRESENTED IN GREEN.

Methods	$L_2 \downarrow$	CMR(T)(%) $\uparrow$					Params(M)	FLOPs(G)	Average time(ms)
		$T = 1$	$T = 2$	$T = 3$	$T = 4$	$T = 5$			
UNet [60]	4.39	19.69	37.32	56.43	69.93	79.60	2.44	48.82	8
UNet+MEFL	3.69(-0.7)	23.00(+3.31)	44.52(+7.2)	65.04(+8.61)	77.30(+7.37)	84.91(+5.31)	2.55	216.30	31
TransUNet [61]	4.04	19.93	42.16	62.50	74.59	82.31	210.57	120.44	57
TransUNet+MEFL	3.39(-0.65)	24.35(+4.42)	45.93(+3.77)	65.63(+3.13)	77.18(+2.59)	84.67(+2.36)	210.58	482.61	197
U-transformer [62]	8.16	18.99	36.44	56.72	66.63	74.00	23.36	319.01	55
U-transformer+MEFL	5.92(-2.24)	18.81(-0.18)	38.56(+2.12)	59.20(+2.48)	70.58(+4.28)	78.60(+4.6)	23.37	1276.91	189
Ours	3.39	24.94	48.11	67.92	78.60	85.50	22.14	170.24	123

TABLE VI

ABLATION EXPERIMENTS ON THE NUMBER OF EXPERTS AND FUSION METHOD BASED ON THE OS-256 DATASET. THE TOP TWO VALUES ARE MARKED AS RED AND BLUE, RESPECTIVELY.

Method	$L_2 \downarrow$	CMR(T)(%) $\uparrow$		
		$T = 1$	$T = 2$	$T = 3$
MEFL-0	3.93	20.75	42.28	62.85
MEFL-2	3.70	23.00	43.40	65.04
MEFL-3	3.53	24.65	45.17	66.16
MEFL-4	3.39	24.94	48.11	67.92
MEFL-5	3.41	24.29	46.46	67.04
MEFL-6	3.64	26.18	47.41	67.69
MEFL-S-2(4)	3.69	22.41	44.22	64.86
MEFL-4-A	3.50	24.06	46.52	66.63

and computational costs, this paper employs four experts in the MEFL strategy.

This part also simulates a sparse gated fusion of expert features in MEFL. For example, “MEFL-S-2(4)” indicates that MEFL only selects two expert features from four experts for fusion. In comparison to “MEFL-4”, the results of “MEFL-S-2(4)” in an increase of average  $L_2$  by 0.3 and a decrease in CMR(3) by 3.06%. Therefore, we focus on integrating knowledge from all experts to enrich feature representation and enhance feature discriminability. Additionally, we compare our soft router dynamic fusion method and the hard gating expert feature fusion mechanism. “MEFL-4-A” treats all expert features equally. It can be seen that our learnable soft router fusion mechanism performs better than “MEFL-4-A”. Specifically, the average  $L_2$  decreased by 0.11, and CMR(3) increased by 1.29%. This improvement is attributed to each expert focusing on different patterns of features. The learnable soft router selectively filters out task-irrelevant features and fuses important salient features for image registration.

#### H. Influence of the template image size

This section primarily investigates the impact of template image size on the performance of image registration based on the OS and the SEN1-2 datasets. For the OS-256 and SEN1-2 datasets, the reference images size is  $256 \times 256$ , the template image sizes are  $200 \times 200$ ,  $192 \times 192$ ,  $160 \times 160$ ,  $128 \times 128$ , and  $96 \times 96$ , respectively. For the OS-512 dataset, the reference images of size  $512 \times 512$ , template image sizes are  $400 \times 400$ ,

$384 \times 384$ ,  $320 \times 320$ ,  $256 \times 256$ , and  $192 \times 192$ , respectively. As the template image size decreases, the potential matching localization space increases.

Figure 8 presents the registration results of our proposal and F3Net. As the size of the template image increases, the corresponding CMR significantly improves, and average  $L_2$  gradually decreases. For example, as shown in Fig. 8 (a) and (d), when the template image size increases from 96 pixels to 128 pixels, CMR(3) improves by 7.90%, and average  $L_2$  decreases by 43.80%. When the template image size increases from 128 to 160 pixels, CMR(3) increases by 9.44%, and average  $L_2$  decreases by 48.70%. When the template image size increases from 160 to 200 pixels, CMR(3) improves by 8.02%, while average  $L_2$  only decreases by 32.20%. The main reason is that when the template image size is too small, the image lacks sufficient discriminative information, resulting in poor registration accuracy. Meanwhile, when the reference image size is fixed, a smaller template image tends to have a wider spatial matching range, increasing registration difficulty. As the template image size increases, the computational cost also increases.

Additionally, our proposed method significantly outperforms F3Net in registration accuracy under different template image sizes. Moreover, our method is more robust than F3Net to template size changes. For example, as shown in Fig. 8 (b), when the template size decreases from 384 to 320, the CMR(1) of our method decreases by 4.01%, while F3Net decreases by 13.68%; the CMR(2) of our method decreases by 5.42%, while F3Net decreases by 26.89%. As shown in Fig. 8 (e), when the template size decreases from 256 pixels to 192 pixels, the average  $L_2$  of our method increases by 8.72, while F3Net increases by 26.15. These results further demonstrate the robustness of our method, which can stably adapt to templates of different sizes while maintaining good registration accuracy. Furthermore, our method can extract discriminative features from small template images with sparse textures, thereby improving registration performance.

#### I. The effectiveness of MEFL on other frameworks

This section validates the effectiveness of our proposed multi-expert feature learning (MEFL) strategy on other frameworks, such as the CNN-based method of UNet [60], the Transformer-based methods of TransUNet [61] and U-Transformer [62].

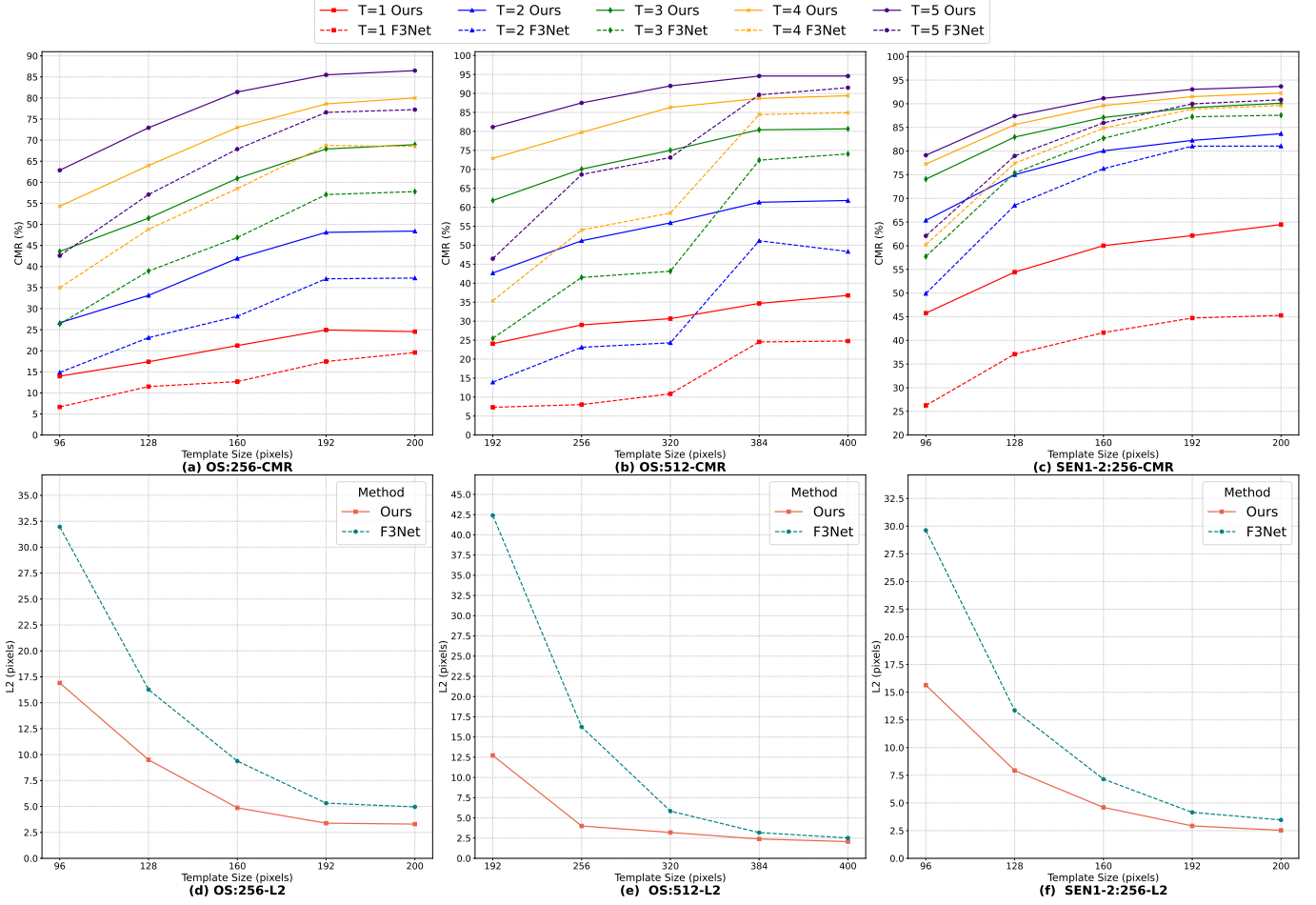


Fig. 8. Registration performances of our RegistrationMamba and F3Net on the OS dataset and SEN1-2 dataset under different template sizes and threshold values.

Firstly, MEFL can effectively improve the image registration performances of various registration frameworks. As shown in Table V, when the MEFL strategy is applied to UNet, the average  $L_2$  decreases by 0.7 (from 4.39 to 3.69), and the CMR(3) improves by 8.61% (from 56.43% to 65.04%). Similarly, when the MEFL strategy is applied to TransUNet, the average  $L_2$  decreases by 0.65 (from 4.04 to 3.39), and the CMR(3) increases by 3.13% (from 62.50% to 65.63%). These results demonstrate that our MEFL strategy is effective and universal, seamlessly integrating into various frameworks and yielding significant performance improvements.

Secondly, Transformer-based frameworks achieve better performances. For example, UNet gets an average  $L_2$  of 4.39 and a CMR(3) of 56.43%. However, TransUNet achieves an average  $L_2$  of 4.04, with a CMR(3) of 62.50%. Compared to UNet, TransUNet benefits from its self-attention mechanism and global receptive field, reducing the average  $L_2$  by 0.35 and improving the CMR(3) by 6.07%. However, Transformer-based frameworks significantly increase computational costs. For example, the number of parameters of UNet is 2.44M, while the number of parameters of TransUNet is 210.57M.

Additionally, our RegistrationMamba has advantages over other methods in terms of registration performance and computation complexity. Our RegistrationMamba achieves an av-

erage  $L_2$  of 3.39 and a CMR(3) of 67.92%. Compared to UNet+MEFL, our method reduces the average  $L_2$  by 0.3 and improves the CMR(3) by 2.88%. Compared to TransUNet+MEFL, our method improves the CMR(3) by 2.29%. Notably, RegistrationMamba achieves optimal performance with only 22.14M network parameters and 170.24G FLOPs. The reason is that RegistrationMamba can efficiently capture global contextual information with linear complexity, achieving good registration performances without expensive computational burdens. Furthermore, the MEFL strategy enhances the richness and discriminability of features, contributing to significant performance gains in images with limited textures.

#### J. Computational efficiency

This section displays the computational efficiency of our method and other image registration approaches based on the SEN 1-2 dataset, as shown in Table V and VII.

Compared with other deep learning-based methods, our proposed method achieves the best performance and lowest time cost. The average registration time on a pair of images of our method is 123 ms and achieves a CMR(3) of 89.20%. DDFN relies on shallow features for registration, and its registration accuracy needs to be further improved, especially when the images have few salient features. FFT U-Net and



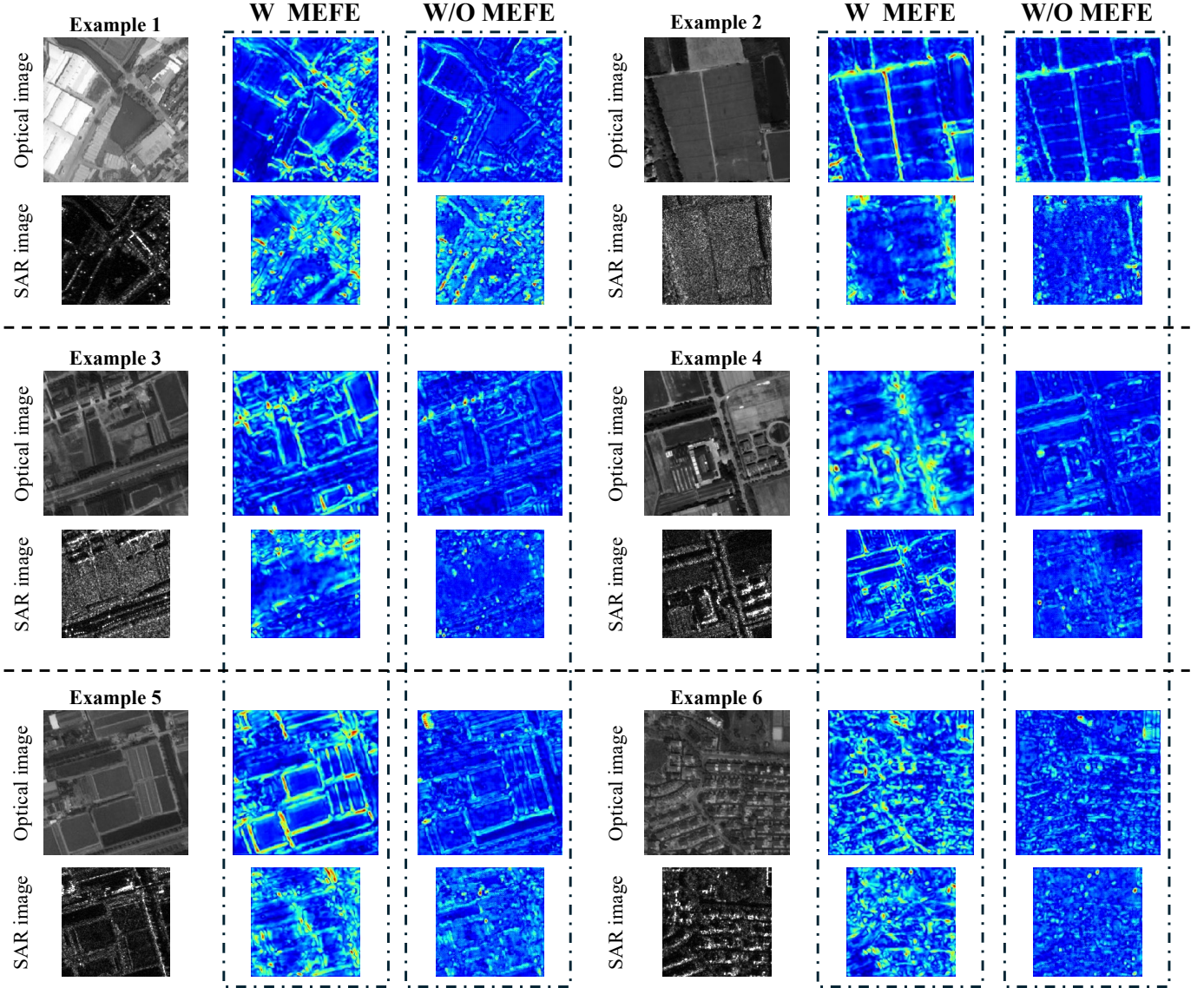


Fig. 9. Feature visualization of optical and SAR images when the deep model with (W) and without (W/O) MEFL strategy.

MARU-Net employ the U-Net framework and leverage the frequency domain for similarity computation, increasing the registration time cost. Although NCC is faster than the more advanced methods, it exhibits the worst performance. This is because NCC directly computes the similarity metric based on the input images, where the cross-modal images display significant differences.

In addition, in Table V, we compare the efficiency of cross-modal image registration based on different frameworks. It can be seen that the CNN-based registration framework has faster inference times than the Transformer-based framework but lower registration performances. For example, the average registration time of UNet+MEFL is 31 ms and its corresponding registration accuracy of CMR(2) is 44.52%, while the average registration time of TransUNet+MEFL is 197 ms and its registration accuracy of CMR(2) is 45.93%. Compared with the Transformer-based framework, our proposed Registration-Mamba has a faster registration speed (123ms for each pair

of images) and better registration performance (CMR(2) is 48.11%). The high computational efficiency and performance of our RegistrationMamba mainly benefit from the following aspects. Firstly, it takes advantage of the parallel optimization capabilities of the Mamba framework, improving efficiency. Secondly, we adopt the GPU to accelerate similarity calculations by using the template image as convolution kernels and convolution with the reference image. Moreover, our approach effectively captures global and local features, achieving high accuracy while achieving rapid inference speeds.

#### K. Visualization

1) *Visualization of features*: This part presents the features of the RegistrationMamba with (W) and without (W/O) the MEFL strategy in Fig. 9. It can be observed that when the deep model uses the MEFL strategy, the features of the optical and SAR images have more distinctive information and sharper boundaries than those without the MEFL strategy. In contrast,

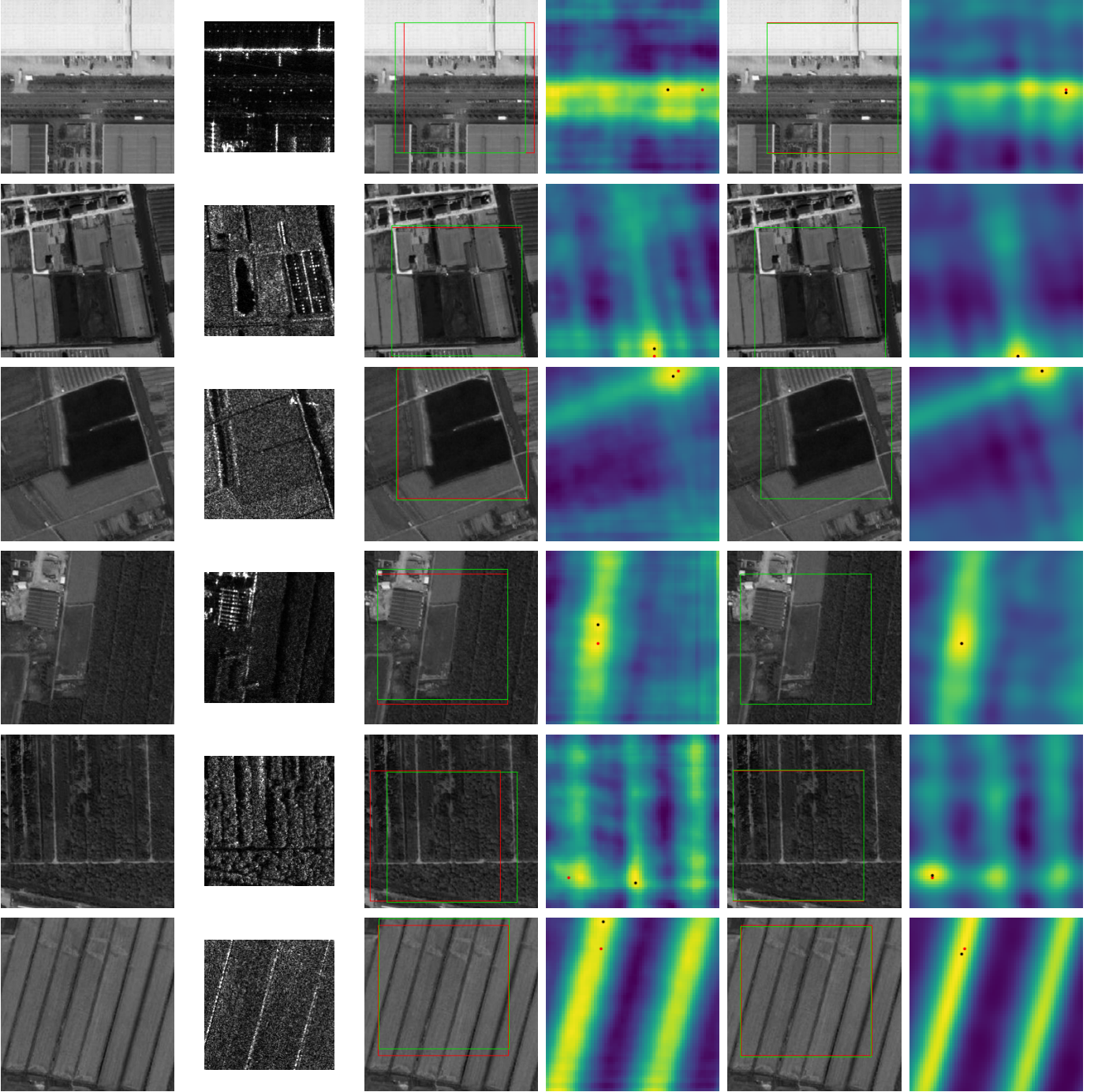


Fig. 10. The visual results of F3Net and our RegistrationMamba on the OS-256 dataset. The first and second columns represent the optical image (reference image) and the corresponding SAR image (template image), respectively. The third and fourth columns are the registration results and similarity maps of F3Net, respectively. The fifth and sixth columns represent the registration results and similarity maps of RegistrationMamba, respectively.

when the MEFL strategy is not applied, the features are blurred, especially in images with limited textures. The deep model struggles to effectively extract enough discriminative information for matching and registration, ultimately impairing registration performance. These visualization results show that our proposed MEFL can encourage the deep module to explore rich features for more accurate registration. MEFL employs various experts to extract image features from different perspectives and uses a learnable soft router for adaptive feature aggregation. Therefore, MEFL can extract rich discriminative

information from images with poor textures and significantly improve the registration performances.

2) *Visualization of registration results*: This part visualizes cross-modal image registration results and corresponding similarity maps of our proposal and F3Net, as shown in Fig. 10. In the optical image, the red and green boxes represent the ground-truth and predicted matching positions, respectively. We also show the similarity map of features across images, where the red and black dots indicate the ground-truth and predicted matching coordinates, respectively.



TABLE VII

THE AVERAGE REGISTRATION TIME OF A PAIR OF IMAGES AND CMR(3) OF EXISTING METHODS ON THE SEN1-2 DATASET. THE TOP TWO VALUES ARE MARKED AS RED AND BLUE.

Model	Average time(ms) ↓	CMR(3)(%) ↑
NCC [7]	57	5.00
MI [8]	5450	54.00
DDFN [34]	239	50.00
Siamese CNN [12]	629	72.00
FFT U-Net [37]	437	74.00
MARU-Net [14]	396	82.00
Ours	123	89.20

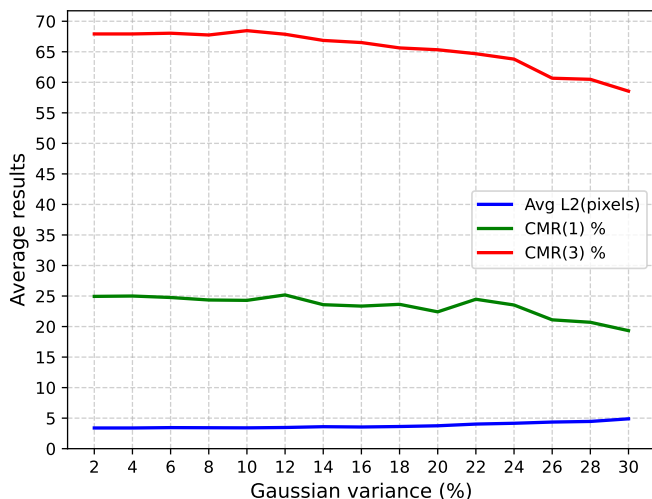


Fig. 11. The performances of RegistrationMamba under different levels of Gaussian noise.

Firstly, from the similarity maps, we can observe that F3Net tends to generate multiple peaks of high similarity responses, whereas our method suppresses similarity values in non-matching areas and maintains an unimodal similarity peak in the registration regions. Secondly, our method can accurately register images with weak and local repeated textures (see the fourth and fifth samples). F3Net produces multiple high similarity peaks and finds a rough matching position. In contrast, our method predicts positions with smaller errors, even precisely locating the true position. This is because our method integrates global context information and local features, enhancing the feature discrimination and improving the registration performances of images with weak and local repeated textures. However, our proposal and F3Net should improve the registration performance in extreme and challenging cases. For example, in the sixth sample, we observe that the optical image contains few textures, and its local features are highly similar and repeatable, which will lead to multiple high responses in the similarity map and mismatching results.

#### L. Robustness analysis

In this section, we analyze the sensitivity of the proposed method to noise based on the OS dataset. The optical images in the OS dataset are added to different levels of Gaussian

white noise with a mean of 0 and variance from 2% to 30%. We present their registration results of CMR (with  $T = 1$  and  $T = 3$ ) and average  $L_2$ . As shown in Fig. 11, when the image noise variance increases from 2% and 20%, although our method is not trained on the noised images, the registration performances are relatively stable. When the Gaussian noise variance exceeds 22%, the registration performance decreases slightly. These experimental results indicate that our proposal is robust to noise. The main reason is that the Mamba-based model and the MEFL strategy enhance salient feature learning and handle challenging scenarios effectively.

#### V. CONCLUSION

This paper proposes a novel RegistrationMamba with multi-expert feature learning for cross-modal remote sensing image registration. We first introduce the Mamba framework into image registration, which can efficiently capture global contextual features in the images with slight computational complexity by employing a multi-directional cross-scanning strategy. Additionally, this paper proposes a multi-expert feature learning (MEFL) strategy to further enhance the registration performance on images with limited textures. MEFL leverages multiple feature experts to extract discriminative information from various augmented images and employs a learnable soft router to fuse the features from multiple experts dynamically. MEFL can be seamlessly integrated into various frameworks, significantly boosting registration performance. Furthermore, we integrate an MFA module to extract fine-grained local information, facilitating effective interaction between global and local features and improving registration accuracy. RegistrationMamba effectively alleviates the cross-modal image registration in scenes with limited textures. However, for image scenes with extremely sparse textures and repeated textures, the performances of RegistrationMamba need to be further improved. In the future, we will combine the advantages of different registration frameworks to enhance the richness and discriminability of features and deal with these challenging image scenes.

#### REFERENCES

- [1] X. Geng, L. Jiao, L. Li, X. Liu, F. Liu, and S. Yang, "Fast and effective: Progressive hierarchical fusion classification for remote sensing images," *IEEE Transactions on Multimedia*, vol. 26, pp. 9776–9789, 2024.
- [2] R. Zhou, D. Quan, S. Wang, C. Lv, X. Cao, J. Chanussot, Y. Li, and L. Jiao, "A unified deep learning network for remote sensing image registration and change detection," *IEEE Transactions on Geoscience and Remote Sensing*, vol. 62, pp. 1–16, 2024.
- [3] H. Zhang, W. Ni, W. Yan, D. Xiang, J. Wu, X. Yang, and H. Bian, "Registration of multimodal remote sensing image based on deep fully convolutional neural network," *IEEE Journal of Selected Topics in Applied Earth Observations and Remote Sensing*, vol. 12, no. 8, pp. 3028–3042, 2019.
- [4] S. Wang, D. Quan, X. Liang, M. Ning, Y. Guo, and L. Jiao, "A deep learning framework for remote sensing image registration," *ISPRS Journal of Photogrammetry and Remote Sensing*, vol. 145, pp. 148–164, 2018.
- [5] D. G. Lowe, "Distinctive image features from scale-invariant keypoints," *International journal of computer vision*, vol. 60, pp. 91–110, 2004.
- [6] C. Lv, W. Wang, D. Quan, S. Wang, L. Dong, X. Jiang, Y. Gu, and L. Jiao, "Fourier domain adaptive multi-modal remote sensing image template matching based on siamese network," in *IGARSS 2024-2024 IEEE International Geoscience and Remote Sensing Symposium*. IEEE, 2024, pp. 7325–7329.

- [7] K. Briechle and U. D. Hanebeck, "Template matching using fast normalized cross correlation," in *Optical pattern recognition XII*, vol. 4387. SPIE, 2001, pp. 95–102.
- [8] J. Inglada and A. Giros, "On the possibility of automatic multisensor image registration," *IEEE Transactions on Geoscience and Remote Sensing*, vol. 42, no. 10, pp. 2104–2120, 2004.
- [9] Y. Ye and L. Shen, "Hopc: A novel similarity metric based on geometric structural properties for multi-modal remote sensing image matching," *ISPRS Annals of the Photogrammetry, Remote Sensing and Spatial Information Sciences*, vol. 3, pp. 9–16, 2016.
- [10] Y. Ye, L. Bruzzone, J. Shan, F. Bovolo, and Q. Zhu, "Fast and robust matching for multimodal remote sensing image registration," *IEEE Transactions on Geoscience and Remote Sensing*, vol. 57, no. 11, pp. 9059–9070, 2019.
- [11] S. Li, Z. Wang, Z. Liu, C. Tan, H. Lin, D. Wu, Z. Chen, J. Zheng, and S. Z. Li, "Moganet: Multi-order gated aggregation network," in *The Twelfth International Conference on Learning Representations*, 2023.
- [12] N. Merkle, W. Luo, S. Auer, R. Müller, and R. Urtasun, "Exploiting deep matching and sar data for the geo-localization accuracy improvement of optical satellite images," *Remote Sensing*, vol. 9, no. 6, p. 586, 2017.
- [13] W. Wu, Y. Xian, J. Su, and L. Ren, "A siamese template matching method for sar and optical image," *IEEE Geoscience and Remote Sensing Letters*, vol. 19, pp. 1–5, 2021.
- [14] M. Gazzea, O. Sommervold, and R. Arghandeh, "Maru-net: Multiscale attention gated residual u-net with contrastive loss for sar-optical image matching," *IEEE Journal of Selected Topics in Applied Earth Observations and Remote Sensing*, vol. 16, pp. 4891–4899, 2023.
- [15] H. Zhang, Y. Yue, H. Li, P. Liu, Y. Jia, W. He, and Z. Wang, "Shared contents alignment across multiple granularities for robust sar-optical image matching," *Information Fusion*, vol. 106, p. 102298, 2024.
- [16] Z. Fan, Y. Pi, M. Wang, Y. Kang, and K. Tan, "Gls-mift: A modality invariant feature transform with global-to-local searching," *Information Fusion*, vol. 105, p. 102252, 2024.
- [17] D. Quan, Z. Wang, S. Wang, Y. Li, B. Ren, M. Kang, J. Chanussot, and L. Jiao, "F3net: Adaptive frequency feature filtering network for multimodal remote sensing image registration," *IEEE Transactions on Geoscience and Remote Sensing*, vol. 62, pp. 1–13, 2024.
- [18] Y. Ye, C. Yang, G. Gong, P. Yang, D. Quan, and J. Li, "Robust optical and sar image matching using attention-enhanced structural features," *IEEE Transactions on Geoscience and Remote Sensing*, vol. 62, pp. 1–12, 2024.
- [19] Y. Liu, H. Qi, and S. Peng, "Optical and sar images matching based on phase structure convolutional features," *IEEE Geoscience and Remote Sensing Letters*, 2023.
- [20] A. Gu and T. Dao, "Mamba: Linear-time sequence modeling with selective state spaces," *arXiv preprint arXiv:2312.00752*, 2023.
- [21] Q. Liu, J. Yue, Y. Fang, S. Xia, and L. Fang, "Hypermamba: A spectral-spatial adaptive mamba for hyperspectral image classification," *IEEE Transactions on Geoscience and Remote Sensing*, 2024.
- [22] H. Chen, J. Song, C. Han, J. Xia, and N. Yokoya, "Changemamba: Remote sensing change detection with spatio-temporal state space model," *IEEE Transactions on Geoscience and Remote Sensing*, 2024.
- [23] W. Cai, J. Jiang, F. Wang, J. Tang, S. Kim, and J. Huang, "A survey on mixture of experts," *arXiv preprint arXiv:2407.06204*, 2024.
- [24] J. Puigcerver, C. Riquelme, B. Mustafa, and N. Houlsby, "From sparse to soft mixtures of experts," *arXiv preprint arXiv:2308.00951*, 2023.
- [25] M. N. R. Chowdhury, S. Zhang, M. Wang, S. Liu, and P.-Y. Chen, "Patch-level routing in mixture-of-experts is provably sample-efficient for convolutional neural networks," in *International Conference on Machine Learning*. PMLR, 2023, pp. 6074–6114.
- [26] W. Xu, H. Jiang, and X. Liang, "Leveraging knowledge of modality experts for incomplete multimodal learning," in *Proceedings of the 32nd ACM International Conference on Multimedia*, 2024, pp. 438–446.
- [27] J. Li, Q. Hu, and M. Ai, "Rift: Multi-modal image matching based on radiation-variation insensitive feature transform," *IEEE Transactions on Image Processing*, vol. 29, pp. 3296–3310, 2019.
- [28] S. Suri and P. Reinartz, "Mutual-information-based registration of terrasars-x and ikonos imagery in urban areas," *IEEE Transactions on Geoscience and Remote Sensing*, vol. 48, no. 2, pp. 939–949, 2009.
- [29] R. Li, S. Zheng, C. Zhang, C. Duan, J. Su, L. Wang, and P. M. Atkinson, "Multiattention network for semantic segmentation of fine-resolution remote sensing images," *IEEE Transactions on Geoscience and Remote Sensing*, vol. 60, pp. 1–13, 2021.
- [30] R. Li, S. Zheng, C. Zhang, C. Duan, L. Wang, and P. M. Atkinson, "Abcnet: Attentive bilateral contextual network for efficient semantic segmentation of fine-resolution remotely sensed imagery," *ISPRS journal of photogrammetry and remote sensing*, vol. 181, pp. 84–98, 2021.
- [31] X. Ma, X. Zhang, and M.-O. Pun, "A crossmodal multiscale fusion network for semantic segmentation of remote sensing data," *IEEE Journal of Selected Topics in Applied Earth Observations and Remote Sensing*, vol. 15, pp. 3463–3474, 2022.
- [32] A. Mishchuk, D. Mishkin, F. Radenovic, and J. Matas, "Working hard to know your neighbor's margins: Local descriptor learning loss," *Advances in neural information processing systems*, vol. 30, 2017.
- [33] L. H. Hughes, D. Marcos, S. Lobry, D. Tuia, and M. Schmitt, "A deep learning framework for matching of sar and optical imagery," *ISPRS Journal of Photogrammetry and Remote Sensing*, vol. 169, pp. 166–179, 2020.
- [34] H. Zhang, L. Lei, W. Ni, T. Tang, J. Wu, D. Xiang, and G. Kuang, "Optical and sar image matching using pixelwise deep dense features," *IEEE Geoscience and Remote Sensing Letters*, vol. 19, pp. 1–5, 2020.
- [35] D. Quan, X. Liang, S. Wang, S. Wei, Y. Li, N. Huyen, and L. Jiao, "Afd-net: Aggregated feature difference learning for cross-spectral image patch matching," in *Proceedings of the IEEE/CVF International Conference on Computer Vision*, 2019, pp. 3017–3026.
- [36] D. Quan, H. Wei, S. Wang, Y. Li, J. Chanussot, Y. Guo, B. Hou, and L. Jiao, "Efficient and robust: A cross-modal registration deep wavelet learning method for remote sensing images," *IEEE Journal of Selected Topics in Applied Earth Observations and Remote Sensing*, vol. 16, pp. 4739–4754, 2023.
- [37] Y. Fang, J. Hu, C. Du, Z. Liu, and L. Zhang, "Sar-optical image matching by integrating siamese u-net with fft correlation," *IEEE Geoscience and Remote Sensing Letters*, vol. 19, pp. 1–5, 2021.
- [38] Y. Ye, T. Tang, B. Zhu, C. Yang, B. Li, and S. Hao, "A multiscale framework with unsupervised learning for remote sensing image registration," *IEEE Transactions on Geoscience and Remote Sensing*, vol. 60, pp. 1–15, 2022.
- [39] L. Zhu, B. Liao, Q. Zhang, X. Wang, W. Liu, and X. Wang, "Vision mamba: Efficient visual representation learning with bidirectional state space model," *arXiv preprint arXiv:2401.09417*, 2024.
- [40] Y. Xiao, Q. Yuan, K. Jiang, Y. Chen, Q. Zhang, and C.-W. Lin, "Frequency-assisted mamba for remote sensing image super-resolution," *IEEE Transactions on Multimedia*, vol. 27, pp. 1783–1796, 2025.
- [41] X. Huang, Y. Zhang, F. Luo, and Y. Dong, "Dynamic token augmentation mamba for cross-scene classification of hyperspectral image," *IEEE Transactions on Geoscience and Remote Sensing*, 2024.
- [42] Z. Dong, G. Yuan, Z. Hua, and J. Li, "Conmamba: Cnn and ssm high-performance hybrid network for remote sensing change detection," *IEEE Transactions on Geoscience and Remote Sensing*, 2024.
- [43] Z. Zhang, X. Fan, X. Wang, Y. Qin, and J. Xia, "A novel remote sensing image change detection approach based on multi-level state space model," *IEEE Transactions on Geoscience and Remote Sensing*, 2024.
- [44] S. Zhao, H. Chen, X. Zhang, P. Xiao, L. Bai, and W. Ouyang, "Rs-mamba for large remote sensing image dense prediction," *IEEE Transactions on Geoscience and Remote Sensing*, 2024.
- [45] B. Pan, Y. Shen, H. Liu, M. Mishra, G. Zhang, A. Oliva, C. Raffel, and R. Panda, "Dense training, sparse inference: Rethinking training of mixture-of-experts language models," *arXiv preprint arXiv:2404.05567*, 2024.
- [46] T. Wei, B. Zhu, L. Zhao, C. Cheng, B. Li, W. Lü, P. Cheng, J. Zhang, X. Zhang, L. Zeng *et al.*, "Skywork-moe: A deep dive into training techniques for mixture-of-experts language models," *arXiv preprint arXiv:2406.06563*, 2024.
- [47] Y. Zhou, N. Du, Y. Huang, D. Peng, C. Lan, D. Huang, S. Shakeri, D. So, A. M. Dai, Y. Lu *et al.*, "Brainformers: Trading simplicity for efficiency," in *International conference on machine learning*. PMLR, 2023, pp. 42 531–42 542.
- [48] B. Chen, K. Chen, M. Yang, Z. Zou, and Z. Shi, "Heterogeneous mixture of experts for remote sensing image super-resolution," *arXiv preprint arXiv:2502.09654*, 2025.
- [49] H. Lin, D. Hong, S. Ge, C. Luo, K. Jiang, H. Jin, and C. Wen, "Rs-moe: A vision-language model with mixture of experts for remote sensing image captioning and visual question answering," *IEEE Transactions on Geoscience and Remote Sensing*, 2025.
- [50] B. Cao, Y. Sun, P. Zhu, and Q. Hu, "Multi-modal gated mixture of local-to-global experts for dynamic image fusion," in *Proceedings of the IEEE/CVF international conference on computer vision*, 2023, pp. 23 555–23 564.
- [51] W. Sun, Y. Tan, J. Li, S. Hou, X. Li, Y. Shao, Z. Wang, and B. Song, "Hotmoe: Exploring sparse mixture-of-experts for hyperspectral object tracking," *IEEE Transactions on Multimedia*, 2025.



- [52] H. Shen, H. Ding, Y. Zhang, X. Cong, Z.-Q. Zhao, and X. Jiang, "Spatial-frequency adaptive remote sensing image dehazing with mixture of experts," *IEEE Transactions on Geoscience and Remote Sensing*, 2024.
- [53] Y. Liu, Y. Tian, Y. Zhao, H. Yu, L. Xie, Y. Wang, Q. Ye, and Y. Liu, "Vmamba: Visual state space model," *arXiv preprint arXiv:2401.10166*, 2024.
- [54] Y. Zhou, T. Lei, H. Liu, N. Du, Y. Huang, V. Zhao, A. M. Dai, Q. V. Le, J. Laudon *et al.*, "Mixture-of-experts with expert choice routing," *Advances in Neural Information Processing Systems*, vol. 35, pp. 7103–7114, 2022.
- [55] M. Schmitt, L. H. Hughes, and X. X. Zhu, "The sen1-2 dataset for deep learning in sar-optical data fusion," *arXiv preprint arXiv:1807.01569*, 2018.
- [56] Y. Xiang, R. Tao, F. Wang, H. You, and B. Han, "Automatic registration of optical and sar images via improved phase congruency model," *IEEE Journal of Selected Topics in Applied Earth Observations and Remote Sensing*, vol. 13, pp. 5847–5861, 2020.
- [57] H. Xu, M. He, Z. Rao, and W. Li, "Him-net: A new neural network approach for sar and optical image template matching," in *2021 IEEE International Conference on Image Processing (ICIP)*. IEEE, 2021, pp. 3827–3831.
- [58] B. Li, L. Y. Wu, D. Liu, H. Chen, Y. Ye, and X. Xie, "Image template matching via dense and consistent contrastive learning," in *2023 IEEE International Conference on Multimedia and Expo (ICME)*. IEEE, 2023, pp. 1319–1324.
- [59] J. P. Pluim, J. A. Maintz, and M. A. Viergever, "Mutual-information-based registration of medical images: a survey," *IEEE transactions on medical imaging*, vol. 22, no. 8, pp. 986–1004, 2003.
- [60] O. Ronneberger, P. Fischer, and T. Brox, "U-net: Convolutional networks for biomedical image segmentation," in *Medical image computing and computer-assisted intervention—MICCAI 2015: 18th international conference, Munich, Germany, October 5-9, 2015, proceedings, part III 18*. Springer, 2015, pp. 234–241.
- [61] J. Chen, Y. Lu, Q. Yu, X. Luo, E. Adeli, Y. Wang, L. Lu, A. L. Yuille, and Y. Zhou, "Transunet: Transformers make strong encoders for medical image segmentation," *arXiv preprint arXiv:2102.04306*, 2021.
- [62] O. Petit, N. Thome, C. Rambour, L. Themyr, T. Collins, and L. Soler, "U-net transformer: Self and cross attention for medical image segmentation," in *Machine Learning in Medical Imaging: 12th International Workshop, MLMI 2021, Held in Conjunction with MICCAI 2021, Strasbourg, France, September 27, 2021, Proceedings 12*. Springer, 2021, pp. 267–276.